KeA1

CHINESE ROOTS
GLOBAL IMPACT

Contents lists available at ScienceDirect

Petroleum Science

journal homepage: www.keaipublishing.com/en/journals/petroleum-science

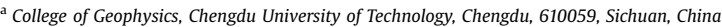


Original Paper

Viscoacoustic generalized screen propagator in constant-Q model

Zhong-Kui Dai ^a, Jia-Chun You ^{a, *}, Xing-Guo Huang ^b, Wei Liu ^a





^b College of Instrumentation and Electrical Engineering, Jilin University, Changchun, 130021, Jilin, China



ARTICLE INFO

Article history:
Received 6 November 2023
Received in revised form
19 February 2024
Accepted 14 March 2024
Available online 15 March 2024

Edited by Meng-Jiao Zhou

Keywords:

One-way wave equation Viscoacoustic wave equation Generalized screen propagator Attenuation and dispersion effects

ABSTRACT

When seismic waves propagate through the geological formation, there is a significant loss of energy and a decrease in imaging resolution, because of the viscoacoustic properties of subsurface medium. This profoundly impacts seismic wavefield propagation, imaging and interpretation. To accurately image the true structure of subsurface medium, the consensus among geophysicists is to no longer treat subsurface medium as ideal homogeneous medium, but rather to incorporate the viscoacoustic properties of subsurface medium. Based on the generalized screen propagator using conventional acoustic wave equation (acoustic GSP), our developed method introduces viscoacoustic compensation strategy, and derives a one-way wave generalized screen propagator based on time-fractional viscoacoustic wave equation (viscoacoustic GSP). In numerical experiments, we conducted tests on two-dimensional multi-layer model and the Marmousi model. When comparing with the acoustic GSP using the acoustic data, we found that the imaging results of the viscoacoustic GSP using the viscoacoustic data showed a significant attenuation compensation effect, and achieved imaging results for both algorithms were essentially consistent. However, the imaging results of acoustic GSP using viscoacoustic data showed significant attenuation effects, especially for deep subsurface imaging. This indicates that we have proposed an effective method to compensate the attenuated seismic wavefield. Our application on a set of real seismic data demonstrated that the imaging performance of our proposed method in local areas surpassed that of the conventional acoustic GSP. This suggests that our proposed method holds practical value and can more accurately image real subsurface structures while enhancing imaging resolution compared with the conventional acoustic GSP. Finally, with respect to computational efficiency, we gathered statistics on running time to compare our proposed method with conventional O-RTM, and it is evident that our method exhibits higher computational efficiency. In summary, our proposed viscoacoustic GSP method takes into account the true properties of the medium, still achieves migration results comparable to conventional acoustic GSP.

© 2024 The Authors. Publishing services by Elsevier B.V. on behalf of KeAi Communications Co. Ltd. This is an open access article under the CC BY-NC-ND license (http://creativecommons.org/licenses/by-nc-nd/4.0/).

1. Introduction

Current seismic exploration no longer focuses solely on the accuracy of structural morphology but also strives to obtain reliable information about lithology and physical properties. Amplitude information of seismic waves is increasingly crucial in seismic interpretation and reservoir prediction. This necessitates that seismic imaging technology not only achieves high imaging accuracy but also maintains a certain level of amplitude preservation (Qu et al., 2017, 2021a; Li and Qu, 2022). Pre-stack depth migration technology has evolved from the initial Kirchhoff algorithm to oneway wave migration algorithms (Stolt, 1978; Schneider, 1978), RTM algorithms (Whitmore, 1983; McMechan, 1983; Baysal et al., 1983),

* Corresponding author. E-mail address: youjiachun2009@163.com (J.-C. You). and developed to the two-way wave depth migration algorithms (You et al., 2016). Among these, although its imaging performance of the one-way wave algorithm may not match that of two-way wave methods such as RTM, its significant advantage in computational efficiency makes the one-way wave algorithm still widely applicable, maintaining its research and practical value (de Hoop et al., 2000; Zhang et al., 2003, 2005, 2007; Wu, 2003; Mulder and Plessix, 2004).

The research on one-way wave migration methods can be clearly recalled to 1980s (Claerbout, 1985). Subsequently, phase-shift methods (PS) and phase-shift plus interpolation methods (PSPI) were introduced by Gazdag (1978) and Gazdag and Sguazzero (1984), respectively. Almost at the same time, the split-step Fourier (SSF) and Fourier finite-difference (FFD) migration algorithms were proposed by Stoffa et al. (1990) and Ristow and Rühl (1994), respectively, to deal with imaging of medium

with strong velocity changes. These two migration algorithms demonstrated a good performance of applicability to medium with lateral velocity variations. The introduction of the generalized screen propagator (GSP; Wu, 1994; de Hoop et al., 2000; Le Rousseau and de Hoop, 2001) represents further advancements in one-way wave migration algorithms and phase screen theory. It also accurately describes the propagation of seismic waves in steeply dipping geological formations or complex structures. To meet a broader range of application requirements, the GSP method evolved to involve not only acoustic medium but also transversely isotropic (TTI) medium and elastic medium (Shin et al., 2015; Kim et al., 2016). It has transitioned from using single one-way wave propagators to implementing two-way wave depth migration, significantly expanding the practical application scope of the GSP (You et al., 2018a). Our paper represents a novel attempt to combine the GSP with viscoacoustic medium.

In generally, conventional one-way wave migration methods often rely on approximation theories such as Taylor series or Pade series to calculate vertical wavenumbers, leading to limited imaging angles for strong lateral velocity variations and complex medium, especially in the case of steeply dipping medium. To enhance the imaging capabilities of one-way wave migration methods in complex medium, the wavefield modal expansion techniques and the concept of localized decomposed Beamlet propagator are proposed (Grimbergen et al., 1998; Wu et al., 2000). The optimization algorithm can enhance the SSF and FFD algorithms, improving the imaging angle of the two methods and achieving more accurate 3D depth migration (Liu and Zhang, 2006; Zhang and Liu, 2007; Zhang et al., 2010a). Research has also progressed in the study of computational efficiency, imaging accuracy, and amplitudepreserving capabilities of one-way wave migration algorithms. Such as the synthetic plane wave methods, the matrix decomposition-based one-way wave true amplitude migration algorithm, and the improved higher-order GSP algorithms (Ye et al., 2013; You et al., 2018b; He et al., 2019).

Actually, subsurface medium is not ideal homogeneous medium and does not possess entirely elastic properties. Therefore, in seismic exploration, the propagation of seismic waves in the subsurface frequently experiences energy attenuation and dispersion phenomena (Bai et al., 2013; Chen et al., 2023). Conventional prestack acoustic migration does not take into account the compensation of amplitude and phase during the imaging. As the complexity of exploration targets increases, along with the depth and difficulty of exploration, this issue urgently needs to be addressed (Dvorkin and Mavko, 2006; Groby and Tsogka, 2006). To deal with this issue, scholars have conducted extensive research on the absorption and attenuation mechanisms in viscoacoustic medium over the years. Relevant attenuation models can generally be categorized into two types: (1) introducing complex velocity in the frequency domain (Liao and McMechan, 1996; Stekl and Pratt, 1998), and (2) introducing a quality factor Q in the time-domain wave equation (Liu et al., 1976). The time-domain approach typically uses a combination of a series of viscosity parameters, known as standard linear solids, to describe the viscosity of medium. These associated models are called nearly constant-Q (NCQ) models (Lomnitz, 1957; Futterman, 1962; Strick, 1967). In contrast, the Q parameter provided by Liu et al. (1976) is nearly frequencyindependent, and its cutoff parameter is set quite arbitrarily. Therefore, Kjartansson (1979) introduced the constant-Q (CQ) model, where the attenuation factor is a linear function of frequency within the seismic bandwidth, and Q is essentially independent of frequency within the typical frequency band of conventional seismic exploration. Mathematically, CQ model is much simpler than these NCQ models. Based on this, the viscoelastic wave equation is established, which can describe the

propagation of seismic waves in the constant-Q model and enabling wavefield simulations (Carcione et al., 1988, 2002; Robertsson et al.. 1994; Carcione, 2009). The viscoacoustic equation has also been developed. In the viscoacoustic wave equation, the attenuation and dispersion terms are coupled, demanding substantial memory resources for numerical solutions. However, by separating the dispersion term and attenuation term in the coupling equations. the computational efficiency can be significantly improved (Treeby et al., 2010; Treeby and Cox, 2010). In order to enhance the accuracy of viscoelastic wavefield simulations, Dutta and Schuster (2014) used a linearized viscoacoustic modeling operator for forward modeling during the least-squares iterations. Sun et al. (2015) introduced low-rank decomposition methods. Chen et al. (2016) introduced a decoupled fractional Laplacian VWE (viscoacoustic wave equation) using the CQ model. Zhao et al. (2017) used viscoacoustic wave equation to reduce the imaging artifacts and simultaneously proposed compensation operators that are absolutely stable. Qi and Greenhalgh (2019) derived VWE based on generalized standard linear solid model from time domain and frequency domain formulas respectively. Qi and Greenhalgh (2022) employed a weighted function approach to derive VWE related to power-law frequency-dependent Q.

In recent years, there have been significant advancements in viscoacoustic wave equation-based migration. These methods can effectively compensate for seismic absorption and attenuation effects, including viscoacoustic one-way wave migration (Dai and West, 1994), and viscoacoustic RTM (Zhang et al., 2007; Zhu et al., 2014; Qu et al., 2021b). Zhang and Wapenaar (2002) introduced a table-driven explicit operator scheme to image complex twodimensional non-elastic medium. Yu et al. (2002) compensated for seismic wave absorption and attenuation using the split-stepand PSPI-based VWE migration algorithms. Wang (2008) incorporated reverse Q filtering into the one-way wave equation migration process to achieve energy compensation during migration. Zhang et al. (2010b) started from the CQ model for viscoacoustic medium and proposed viscoacoustic wave pseudo-differential equations to make compensation for the attenuation of amplitudes and dispersion of phases. Valenciano et al. (2011) introduced a new FFD scheme of viscoacoustic wave equation migration for wavefield continuous imaging using the NCQ model. Bai et al. (2013) employed a similar approach for attenuation compensation during the Q-RTM process, utilizing a viscoacoustic wave equation with memory-free variables. Zhu and Harris (2014) extended the equation of Treeby et al. (2010) to the field of seismic exploration, proposing the time-domain CQ viscoacoustic wave equation. Zhu et al. (2014) proposed a novel decoupled fractional Laplacian CQ viscoacoustic wave equation, separating the attenuation term into amplitude attenuation and velocity dispersion components. They applied this formulation to Q-compensated viscoacoustic RTM. Dutta and Schuster (2014), as well as Sun and Zhu (2015), compensated for attenuation in least-squares RTM. Based on the work of Zhu and Harris (2014), scholars have developed many strategies for Q-RTM (Sun et al., 2016; Qu et al., 2020; Fathalian et al., 2020; Mu et al., 2022). Qu et al. (2022) proposed a 2D Qcompensated least-squares reverse time migration with velocityanisotropy correction (Q-LSRTM-VA). You et al. (2023) proposed a migration scheme that utilizes Q compensation wavefield extrapolation based on the VWE. This scheme based on time-fractionalorder VWE, achieves efficient wavefield extrapolation in the depth domain. Chen et al. (2023) proposed a Q compensated multicomponent elastic Gaussian beam migration method. Xu et al. (2023) developed several effective improvements for anisotropic attenuation effects in Q-RTM to enhance the imaging quality for complicated structures. Mu et al. (2023) modified the attenuation compensation extrapolation operator and made it only compensate for amplitude loss within the effective frequency band to achieve stable attenuation-compensated RTM.

Currently, research on viscoacoustic wave equations and their applications in seismic exploration and wavefield simulation continues to evolve. Our proposed method represents a novel attempt to combine the GSP with viscoacoustic medium. In the following sections, starting from the VWE, we derived the viscoacoustic generalized screen propagator (viscoacoustic GSP) that incorporates viscoacoustic compensation parameters. We tested the proposed method on two numerical models and a real seismic data. To demonstrate the superiority of our proposed method in terms of imaging performance, we compared the imaging results of the conventional acoustic GSP with acoustic data, viscoacoustic GSP with viscoacoustic data and viscoacoustic GSP with acoustic data. In addition, compared to conventional Q-RTM, our proposed method has advantages in computational efficiency.

2. Theory

2.1. Review of viscoacoustic wave equation

Constant Q viscoacoustic wave equation with fractional Laplacian operator (Kjartansson, 1979) is written as

$$\frac{\partial^{2-2\gamma}p(x,z;t)}{\partial t^{2-2\gamma}} = v^2 \omega_0^{-2\gamma} \nabla^2 p(x,z;t) \tag{1}$$

where p(x,z;t) represents the pressure wave field in the spatial domain, ∇^2 is the Laplace operator, $v^2=c_0^2\cos^2(\pi\gamma/2)$ is defined at the reference frequency ω_0 and the phase velocity c_0 , and the parameter $\gamma=\arctan(1/Q)/\pi$ is a dimensionless quantity, because Q>0, so $0<\gamma<0.5$. When $Q\to\infty$, $\gamma\to0$, the Eq. (1) can be written as acoustic wave equation.

Taking the Fourier transform of Eq. (1), in the frequency domain, it is written as

$$(i\omega)^{2-2\gamma}P(x,z;\omega) = v^2\omega_0^{-2\gamma}\nabla^2P(x,z;\omega)$$
 (2)

where $P(x, z; \omega)$ represents the pressure wave field in the frequency domain.

Therefore, the VWE in frequency-space domain describing a two-dimensional viscoacoustic medium can be written as

$$\frac{\partial^{2} P(x, z; \omega)}{\partial z^{2}} = -\left(\frac{\omega^{2}}{v^{2}} \left(\frac{i\omega}{\omega_{0}}\right)^{-2\gamma} + \frac{\partial^{2}}{\partial x^{2}}\right) P(x, z; \omega) \tag{3}$$

2.2. Viscoacoustic generalized screen propagator

Taking the VWE in a two-dimensional viscoacoustic medium as an example, assuming that the depth direction is the main propagation direction of seismic waves, as seismic waves propagate downward with a certain depth interval, the velocity of the medium varies only laterally within a depth step of Δz . Let $v(x,z_i)$ represent the velocity within the depth interval $(z_i,z_i+\Delta z)$. Eq. (3) can be decomposed as follows:

$$\left(\frac{\partial P(x,z;\omega)}{\partial z} + i\sqrt{\frac{\omega^2}{\nu(x,z_i)^2} \left(\frac{i\omega}{\omega_0}\right)^{-2\gamma} + \frac{\partial^2}{\partial x^2} P(x,z;\omega)}\right) \times \left(\frac{\partial P(x,z;\omega)}{\partial z} - i\sqrt{\frac{\omega^2}{\nu(x,z_i)^2} \left(\frac{i\omega}{\omega_0}\right)^{-2\gamma} + \frac{\partial^2}{\partial x^2} P(x,z;\omega)}\right) \tag{4}$$

The wave equation considering only the downgoing wave is written as

$$\frac{\partial P(x,z;\omega)}{\partial z} = i\sqrt{\frac{\omega^2}{\nu(x,z_i)^2} \left(\frac{i\omega}{\omega_0}\right)^{-2\gamma} + \frac{\partial^2}{\partial x^2}} P(x,z;\omega)$$
 (5)

The solution of Eq. (5) can be written as

$$P(x, z_{i+1}; \omega) = \exp(ik_z \Delta z) P(x, z_i; \omega)$$
(6)

Assuming the background velocity within the $(z_i, z_i + \Delta z)$ interval is c, the corresponding downgoing wave equation is written as

$$\frac{\partial P(x,z;\omega)}{\partial z} = i\sqrt{\frac{\omega^2}{c^2} \left(\frac{i\omega}{\omega_0}\right)^{-2\gamma} + \frac{\partial^2}{\partial x^2}} P(x,z;\omega)$$
 (7)

The square root in Eqs. (5) and (7) represents a generalized differential operator. When performing calculations, we can approximate the square root to various orders by using a Taylor series expansion.

To solve Eq. (5), our definition can be written as

$$k_{z} = \sqrt{\frac{\omega^{2}}{\nu^{2}(x, z_{i})} \left(\frac{i\omega}{\omega_{0}}\right)^{-2\gamma} + \frac{\partial^{2}}{\partial x^{2}}}, k_{z0} = \sqrt{\frac{\omega^{2}}{c^{2}} \left(\frac{i\omega}{\omega_{0}}\right)^{-2\gamma_{0}} + \frac{\partial^{2}}{\partial x^{2}}}$$
(8)

where k_z represents the viscoacoustic vertical wavenumber, k_{z0} represents the reference one.

To facilitate subsequent derivations, we make the following simplification: $v_{\gamma}(x,z_i) = v(x,z_i) \times \left(\frac{i\omega}{\omega_0}\right)^{\gamma}, c_{\gamma_0} = c \times \left(\frac{i\omega}{\omega_0}\right)^{\gamma_0}.$

Then we have

$$k_{z} = \sqrt{\frac{\omega^{2}}{\nu^{2}(x, z_{i})} \left(\frac{i\omega}{\omega_{0}}\right)^{-2\gamma} + \frac{\partial^{2}}{\partial x^{2}}} = \sqrt{\frac{\omega^{2}}{\nu_{\gamma}^{2}(x, z_{i})} + \frac{\partial^{2}}{\partial x^{2}}}$$

$$k_{z0} = \sqrt{\frac{\omega^{2}}{c^{2}} \left(\frac{i\omega}{\omega_{0}}\right)^{-2\gamma_{0}} + \frac{\partial^{2}}{\partial x^{2}}} = \sqrt{\frac{\omega^{2}}{c\gamma_{0}^{2}} + \frac{\partial^{2}}{\partial x^{2}}}$$
(9)

Eq. (9) shares the similar form with the vertical wavenumber of the conventional one-way wave equation. Therefore, the derivation process for the viscoacoustic GSP is consistent with that of the conventional acoustic GSP. Compared with the conventional acoustic GSP, our viscoacoustic GSP defines the velocity as a complex velocity which includes the attenuation and dispersion terms.

To explain the viscoacoustic GSP proposed, we provide a brief derivation.

Here, assuming $s = \frac{1}{\nu_{\gamma}(x,z_i)}$, $s_0 = \frac{1}{c_{\gamma_0}}$, Eq. (9) can be simplified to

$$k_{z0} = \sqrt{\omega^2 s_0^2 - k_x^2} \tag{10}$$

$$k_z = \sqrt{\omega^2 s^2 - k_x^2} = k_{z0} \sqrt{1 - \frac{\omega^2 (s_0^2 - s^2)}{k_{z0}^2}}$$
 (11)

Applying a second-order expansion approximation to the above equation, the viscoacoustic GSP can be obtained:

$$k_{z} = k_{z_{0}} + k_{z_{0}} \sum_{n=1}^{\infty} (-1)^{n} {0.5 \choose n} \left[\left(\frac{\omega^{2} s_{0}^{2}}{\omega^{2} s_{0}^{2} - k_{x}^{2}} \right) \left(\frac{s_{0}^{2} - s^{2}}{s_{0}^{2}} \right) \right]^{n}$$
 (12)

where the specific expression of the binomial is

$$\binom{m}{n} = \frac{m(m-1)\cdots(m-n+1)}{n!} \tag{13}$$

Substituting Eq. (12) into Eq. (6):

$$P(x, z_{i+1}; \omega) = \exp\left(ik_{z0}\Delta z \sum_{n=1}^{\infty} (-1)^n \binom{0.5}{n}\right) \\ \left[\left(\frac{\omega^2 s_0^2}{\omega^2 s_0^2 - k_x^2}\right) \left(\frac{s_0^2 - s^2}{s_0^2}\right)\right]^n \exp(ik_{z0}\Delta z) P(x, z_i; \omega)$$
(12)

The exponential function can be expanded using Taylor series as

$$\exp\left(ik_{z0}\Delta z \sum_{n=1}^{\infty} (-1)^{n} {0.5 \choose n} \left[\left(\frac{\omega^{2} s_{0}^{2}}{\omega^{2} s_{0}^{2} - k_{x}^{2}}\right) \left(\frac{s_{0}^{2} - s^{2}}{s_{0}^{2}}\right) \right]^{n} \right)$$

$$\approx 1 + ik_{z0}\Delta z \sum_{n=1}^{\infty} (-1)^{n} {0.5 \choose n} \left[\left(\frac{\omega^{2} s_{0}^{2}}{\omega^{2} s_{0}^{2} - k_{x}^{2}}\right) \left(\frac{s_{0}^{2} - s^{2}}{s_{0}^{2}}\right) \right]^{n}$$
(15)

Then we can derive the viscoacoustic high-order GSP, which has the similar form to the conventional GSP equation, but has the difference definition in the velocity parameter. In our proposed

Table 1Parameters for wavefield simulation in the viscoacoustic isotropic medium model.

Parameter	Value
Size, m	$2000(z) \times 3500(x)$
Sampling length, s	2.00
Velocity, m/s	2000
Quality factor Q	20
Reference frequency, Hz	1
Sampling interval, s	0.001
Grid spacing, m	$5(z) \times 5(x)$
Source type	Ricker wavelet (dominant frequency of 20 Hz)
Source coordinates, m	(x = 1750, z = 0)

viscoacoustic GSP, we use the complex velocity coupled with viscoacoustic parameters:

$$P(x, z_{i+1}; \omega) = \left(1 + ik_{z0}\Delta z \sum_{n=1}^{\infty} (-1)^n \binom{0.5}{n} \right)$$

$$\left[\left(\frac{\omega^2 s_0^2}{\omega^2 s_0^2 - k_x^2} \right) \left(\frac{s_0^2 - s^2}{s_0^2} \right) \right]^n \exp(ik_{z0}\Delta z) P(x, z_i; \omega)$$
(16)

As the value of n increases, the GSP approximates the propagation behavior of one-way waves in complex medium more closely. Expanding the above equation and substituting each variable, Eq. (16) can be written as

$$\begin{split} &P(x,z_{i+1};\omega) = F_{k_x}^{-1} \big\{ \exp(ik_{z0}\Delta z) F_x[P(x,z_i;\omega)] \big\} + \\ &F_{k_x}^{-1} \Bigg\{ \frac{\exp(ik_{z0}\Delta z)}{\left(1 - c^2 k_x^2 \middle/ \omega^2\right)^{1/2}} F_x \Bigg[\frac{i\omega\Delta z}{2} c_{\gamma_0} \Bigg[\frac{1}{\nu_\gamma^2(x,z_i)} - \frac{1}{c_{\gamma_0}^2} \Bigg] P(x,z_i;\omega) \Bigg] - \\ &\frac{\exp(ik_{z0}\Delta z)}{\left(1 - c^2 k_x^2 \middle/ \omega^2\right)^{3/2}} F_x \Bigg[\frac{i\omega\Delta z}{8} c_{\gamma_0}^3 \Bigg[\frac{1}{\nu_\gamma^2(x,z_i)} - \frac{1}{c_{\gamma_0}^2} \Bigg]^2 P(x,z_i;\omega) \Bigg] + \\ &\frac{\exp(ik_{z0}\Delta z)}{\left(1 - c^2 k_x^2 \middle/ \omega^2\right)^{5/2}} F_x \Bigg[\frac{i\omega\Delta z}{32} c_{\gamma_0}^5 \Bigg[\frac{1}{\nu_\gamma^2(x,z_i)} - \frac{1}{c_{\gamma_0}^2} \Bigg]^3 P(x,z_i;\omega) \Bigg] - \cdots \Bigg\} \end{split}$$

In Eq. (17), F_X represents the Fourier transform with respect to x, while $F_{k_x}^{-1}$ represents the inverse Fourier transform with respect to k_x .

By varying the n value, different-order GSPs can be obtained. Higher values of n result in higher computational precision, but the computational complexity also increases with the order.

We also derived the decoupled viscoacoustic wave equation and

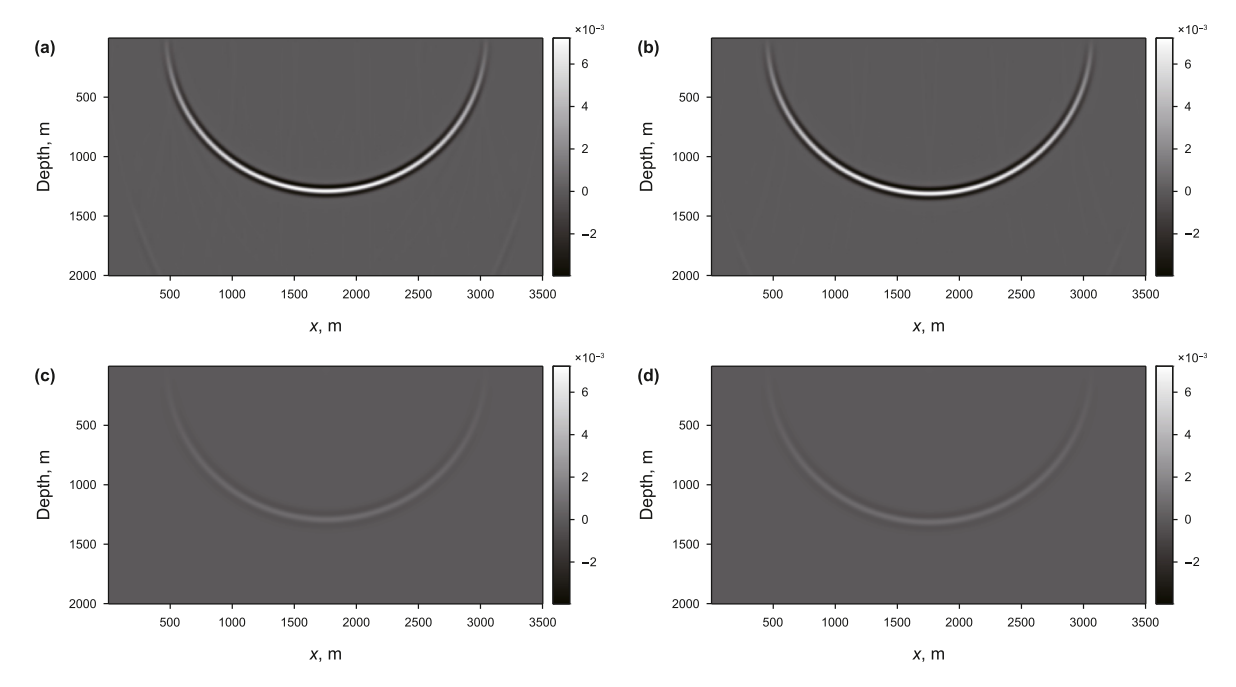
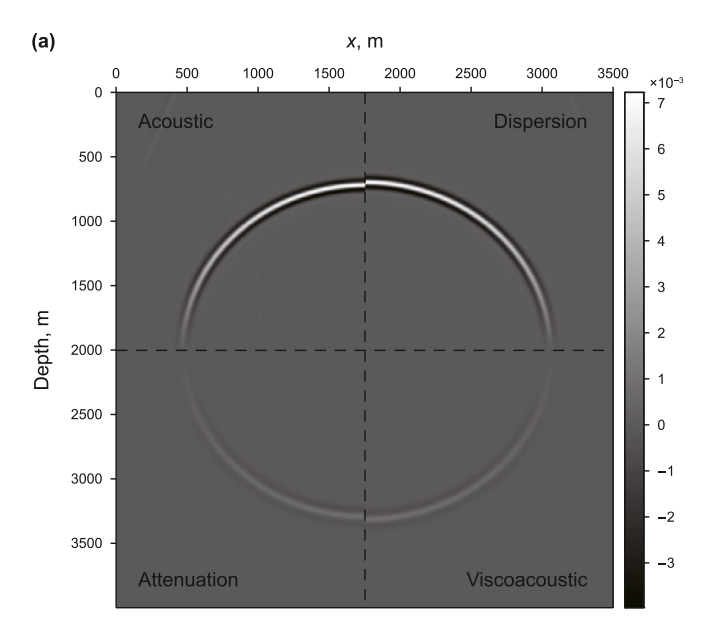
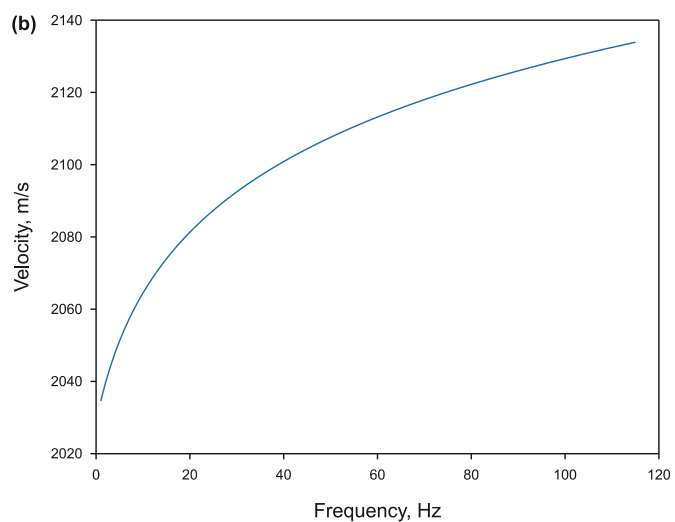


Fig. 1. Snapshots of the wavefield at t = 700 ms in the isotropic model using: (a) acoustic GSP; (b) viscoacoustic GSP considering only the dispersion term; (c) viscoacoustic GSP considering only the sttenuation term; (d) viscoacoustic GSP simultaneously considering attenuation and dispersion terms.





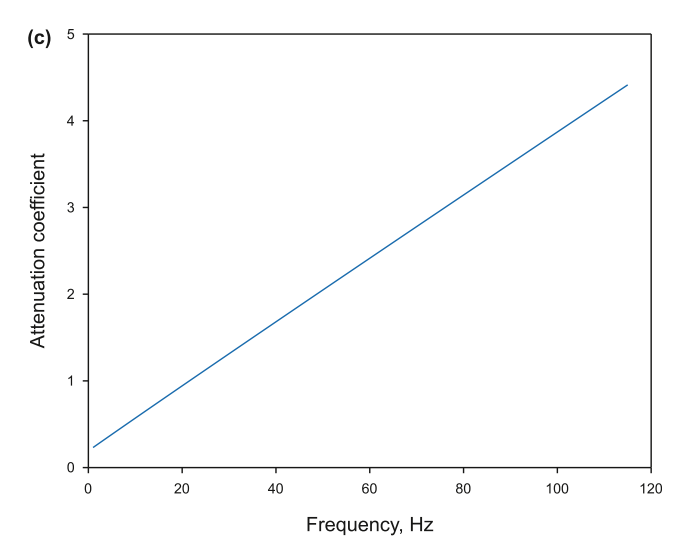


Fig. 2. (a) Wavefields from the acoustic medium and different scenarios of viscoacoustic media (reference frequency: 1 Hz); (b) velocity dispersive curve with frequency (reference frequency: 1 Hz); (c) attenuation curve with frequency (reference frequency: 1 Hz).

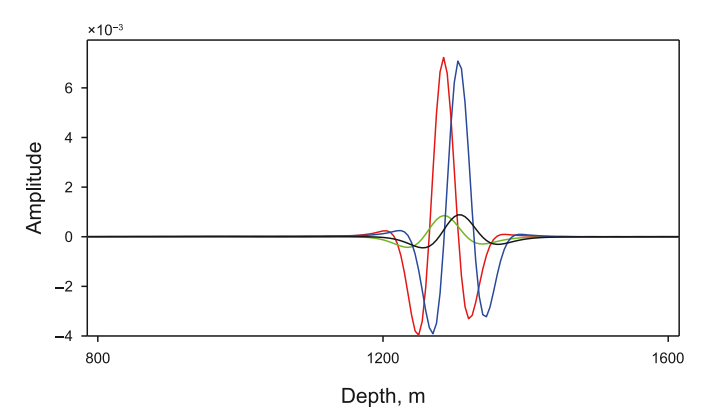


Fig. 3. Waveform comparison by using four algorithms at x=1750 m: red line calculated by the acoustic GSP, blue line calculated by viscoacoustic GSP considering only the dispersion term, green line calculated by viscoacoustic GSP considering only the attenuation term, black line calculated by the full viscoacoustic GSP simultaneously considers attenuation and dispersion term.

its corresponding generalized screen propagator. Applying Euler's formula $i^{2\gamma}=\cos(\pi\gamma)+i\sin(\pi\gamma)$ to Eq. (2), the VWE can be expanded as

$$-\omega^{2}P(x,z;\omega) = \omega^{2\gamma}c^{2}\omega_{0}^{-2\gamma}\cos(\pi\gamma)\nabla^{2}P(x,z;\omega) + \omega^{2\gamma}c^{2}\omega_{0}^{-2\gamma}i\sin(\pi\gamma)\nabla^{2}P(x,z;\omega)$$
(18)

Eq. (18) comprises two parts: the real part and the imaginary part. These parts represent the equations accounting for the dispersion and attenuation effects of wavefield extrapolation in viscoacoustic medium, respectively. In the subsequent derivation, the viscoacoustic wave equations that consider only attenuation effects or dispersion effects are derived, to demonstrate that the viscoacoustic properties of the subsurface structure leading to amplitude attenuation and phase dispersion of seismic waves. The theoretical derivations are presented in Appendices A and B.

In the acoustic one-way wave equation depth migration, evanescent wave suppression can be achieved by discarding the imaginary part in the frequency-wavenumber domain. However, our proposed method in viscoacoustic medium requires introducing the imaginary part as an attenuation compensation term. Detailed steps on how our method achieves attenuation compensation are provided in Appendix C. Additionally, due to stability issues associated with the introduction of the imaginary part, we have designed a frequency-wavenumber domain filter to address this issue in Appendix C.

3. Numerical experiment

Due to the presence of attenuation effects in viscoacoustic medium, seismic waves exhibit phenomena such as velocity dispersion and amplitude attenuation during propagation through geological formation. To address this issue, several scholars have utilized viscoacoustic equations for imaging (Mittet et al., 1995). In the theoretical section, we decoupled the viscoacoustic wave equation and derived viscoacoustic GSP that considering only attenuation effects and only dispersion effects (see details in Appendices A and B). To verify that our proposed viscoacoustic GSP indeed encompass both attenuation and dispersion effects, we initially perform impulse response tests in viscoacoustic isotropic medium by using the three viscoacoustic GSP algorithms. Concurrently, we used the result of conventional acoustic GSP method as a reference because the acoustic wave equation does not exhibit attenuation and dispersion effects. Subsequently, we tested our

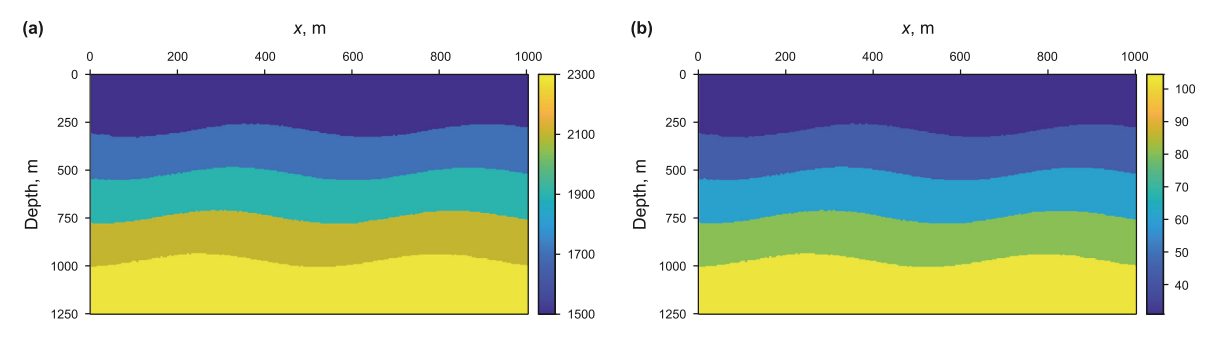


Fig. 4. (a) Velocity model, (b) Q model of the two-dimensional multi-layer model.

Table 2Forward modeling parameters for the two-dimensional multi-layer model.

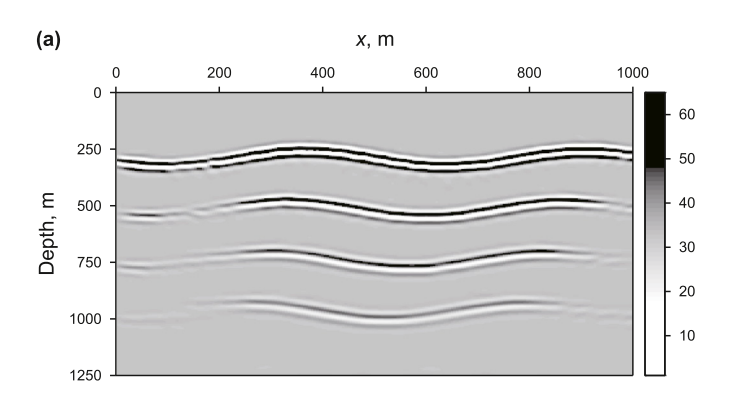
Parameter	Value
Size, m	$1250(z) \times 1000(x)$
Reference frequency, Hz	1
Shot gather number	100
Source interval, m	10
Receiver number	60
Receiver interval, m	5
Minimum offset, m	0
Maximum offset, m	300
Sampling length, s	2.00
Grid spacing, m	$5(z) \times 5(x)$
Sampling interval, s	0.0005
Source type	Ricker wavelet (dominant frequency of 20 Hz)

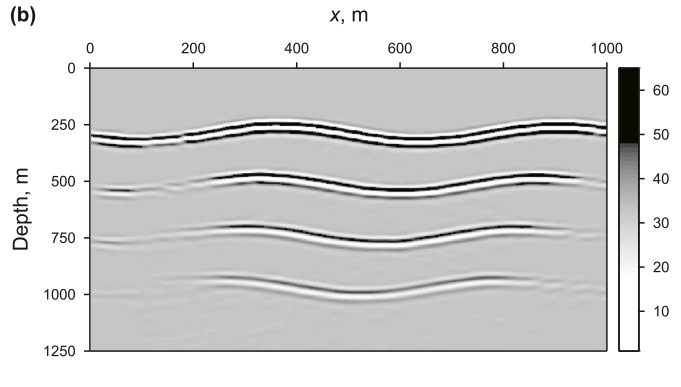
proposed viscoacoustic GSP on two numerical models, the twodimensional multi-layer model and the Marmousi model. The viscoacoustic shot gathers used for migration were obtained by resolving time-fractional viscoacoustic wave equation, while the acoustic shot gathers were obtained by resolving acoustic wave equation, both using finite-difference methods. Finally, we conducted a comparison between the proposed viscoacoustic GSP and the acoustic GSP using actual seismic data. Furthermore, the computational efficiency difference between our proposed method and conventional *O*-RTM is provided for comparison.

3.1. Impulse response in viscoacoustic isotropic medium

According to the introduction above, we achieve (full) viscoacoustic GSP, as well as viscoacoustic GSP considering only the dispersion term or only the attenuation term. This resulted in three one-way viscoacoustic GSP schemes: the (full) viscoacoustic GSP, the viscoacoustic GSP algorithm considering only the dispersion term, and the viscoacoustic GSP algorithm considering only the attenuation term. We conducted impulse response tests on the three viscoacoustic GSP methods, using the result of conventional acoustic GSP as a reference. We conducted simulations of seismic wave propagation in a viscoacoustic isotropic medium model using the four different algorithms. The detailed parameters of the viscoacoustic isotropic model are listed in Table 1. Snapshots of wavefields using the four different algorithms at t = 700 ms are shown in Fig. 1. Fig. 2(a) provides a local comparative analysis of Fig. 1, and the four parts separated by dotted lines come from the above four algorithms, respectively. It is

evident that the wavefields computed using different algorithms exhibit distinct characteristics with clear indications of attenuation and dispersion phenomena. For this example, the velocity dispersion and attenuation curves versus frequency are shown in Fig. 2(b) and (c), respectively, based on Eqs. (C-5) and (C-6). As shown in Fig. 2(b), at a low reference frequency ($f_0 = 1.0 \, \text{Hz}$)





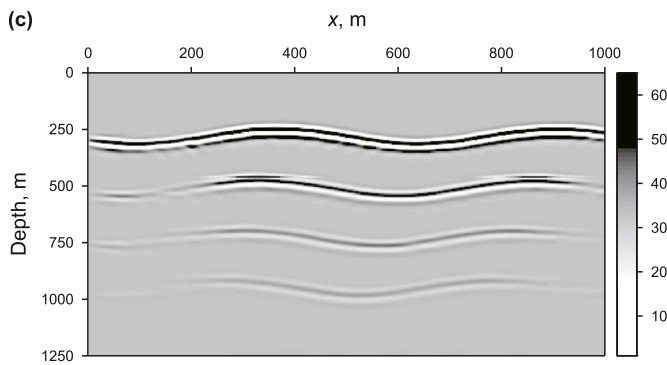
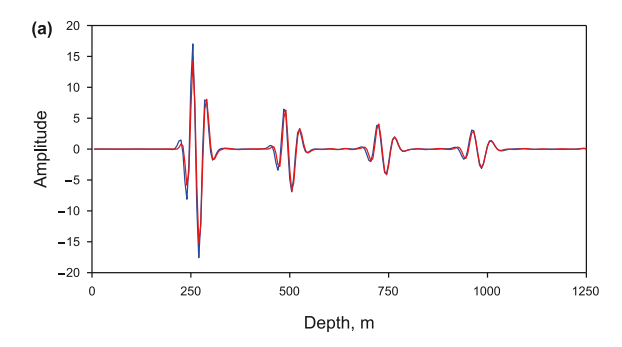


Fig. 5. Imaging results: **(a)** acoustic GSP based on acoustic data, **(b)** viscoacoustic GSP based on viscoacoustic data, **(c)** acoustic GSP based on viscoacoustic data.

in viscoacoustic media, the phase velocity bigger than the background model velocity (2000 m/s). Consequently, the wavefield propagates faster in viscoacoustic media characterized only by phase dispersion. As depicted in Fig. 2(c), the amplitude experiences attenuation in wavefields considering only the effects of



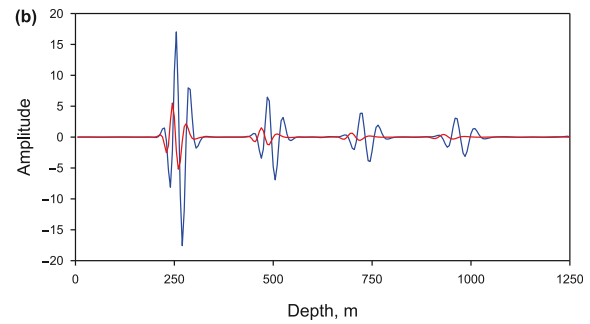
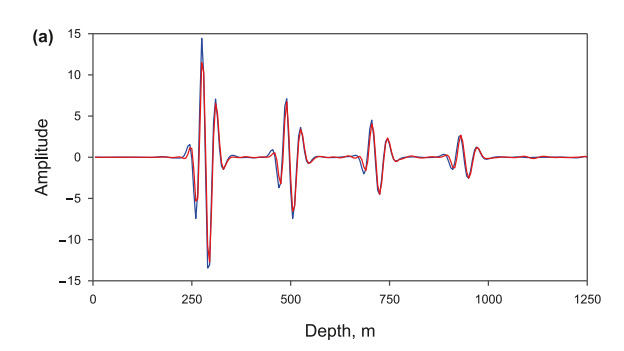


Fig. 6. Comparison of waveforms at x = 400 m. **(a)** Illustration of viscous compensation effect (blue line: acoustic GSP based on acoustic data, red line: viscoacoustic GSP based on viscoacoustic data); **(b)** illustration without compensation (blue line: acoustic GSP based on acoustic data, red line: acoustic GSP based on viscoacoustic data).



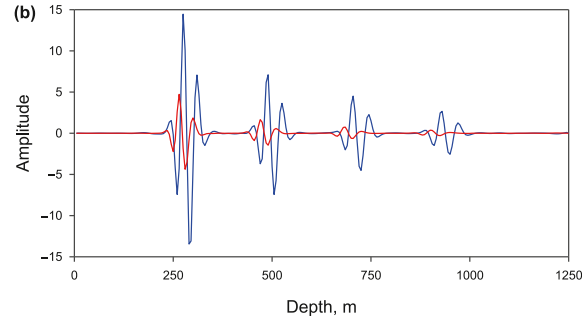


Fig. 7. Comparison of waveforms at x = 800 m, (a) and (b) same as in Fig. 6.

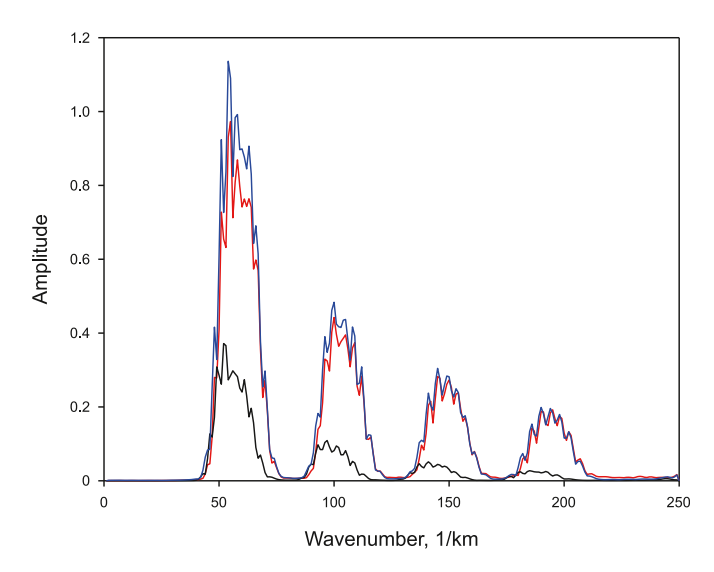


Fig. 8. Normalized average wavenumber spectra of imaging images along the vertical direction: the blue line is calculated by acoustic GSP based on acoustic data, the red line is calculated by viscoacoustic GSP based on viscoacoustic data, and the black line is calculated by acoustic GSP based on viscoacoustic data. All spectral curves are normalized to a reference spectral, which is the spectrum of the acoustic migration from acoustic data, without any attenuation.

amplitude decay (You et al., 2023). To further illustrate the differences in the snapshots obtained using the four algorithms, we have plotted a waveform comparison at $x=1750\,\mathrm{m}$ for the four algorithms shown in Fig. 1. This is depicted in Fig. 3, which demonstrates that the viscoacoustic GSP simultaneously considers attenuation and dispersion effects. This indicates that the derivation of the viscoacoustic GSP is a reasonable and accurate approach, providing a solid foundation for subsequent numerical model

imaging.

3.2. Two-dimensional multi-layer model

To validate the advantages of our proposed method in attenuation compensation, it is applied to the two-dimensional multilayer model. Fig. 4 represents the velocity model and the corresponding quality factor Q (simulated using an empirical formula $Q = 9.73 \times v^{2.85}$; Li, 1993) for the two-dimensional multi-layer models, with detailed model parameters provided in Table 2. Two algorithms, the acoustic GSP and the viscoacoustic GSP, are respectively used for performing wavefield extrapolation and subsequent migration. The final imaging results are displayed in Fig. 5. Taking the imaging of acoustic GSP based on acoustic wave data as reference. It is evident that for the two-dimensional multilayer models, the viscoacoustic GSP based on viscoacoustic data and the acoustic GSP based on acoustic wave data, both accurately image the actual subsurface structures. However, the imaging of the acoustic GSP based on viscoacoustic data exhibits lower imaging energy in the deeper sections. Fig. 5(b) shows the imaging results of our proposed viscoacoustic GSP method using viscoacoustic data. It can be observed that there is some noise present in the deeper parts of the imaging results. This is because during attenuation compensation, the entire wavefield is compensated, leading to the amplification of noise energy and its appearance in the final imaging results. To visually illustrate the compensation performance of viscoacoustic GSP, we select waveforms at x = 400 m, x = 800 m for a comparative display, as shown in Figs. 6 and 7. From Fig. 6(a) and 7(a), it can be observed that the waveforms obtained by viscoacoustic GSP based on viscoacoustic data closely resemble the waveforms obtained by acoustic GSP based on acoustic data, indicating that the viscoacoustic GSP shows a good performance for the attenuation effects. However, Figs. 6(b) and 7(b) show that the imaging results of the acoustic GSP based on

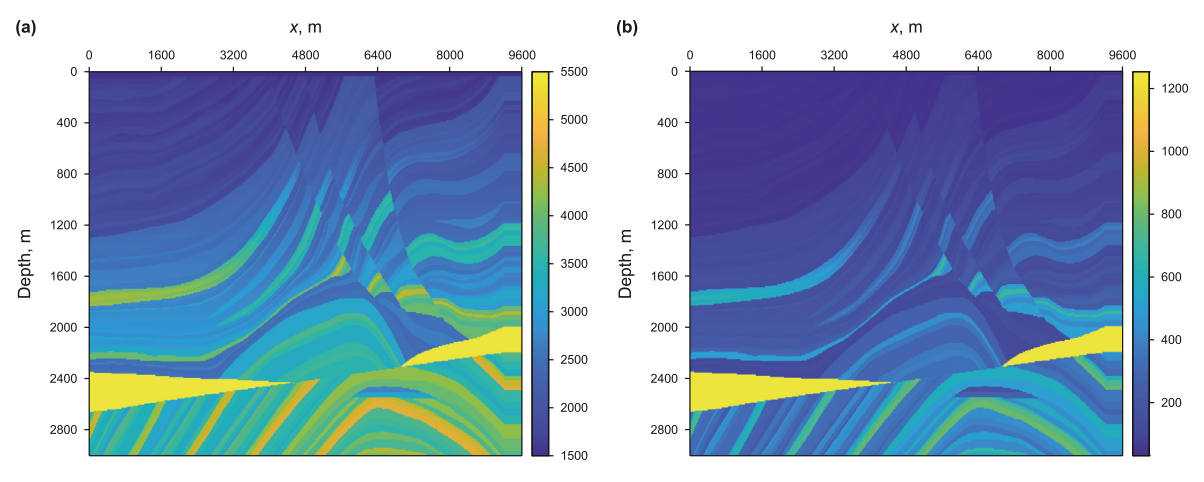


Fig. 9. (a) Velocity model, (b) Q model of the Marmousi model.

Table 3 Forward modeling parameters for the Marmousi model.

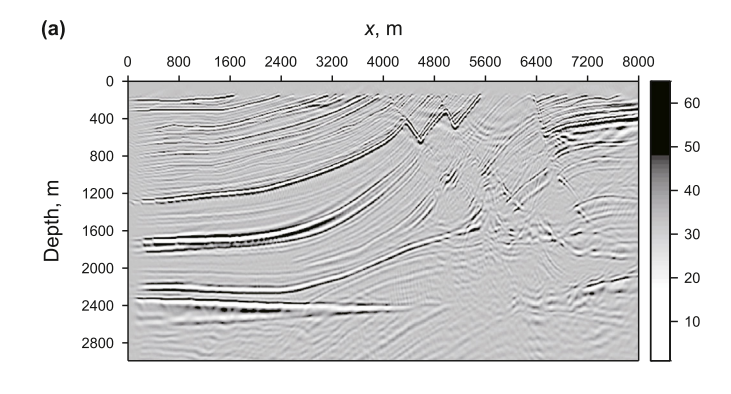
Parameter	Value
Size, m	$3000(z) \times 9600(x)$
Reference frequency, Hz	1
Shot gather number	120
Source interval, m	64
Receiver number	240
Receiver interval, m	8
Minimum offset, m	0
Maximum offset, m	1920
Sampling length, s	3.00
Grid spacing, m	$8(z) \times 8(x)$
Sampling interval, s	0.0005
Source type	Ricker wavelet (dominant frequency of 20 Hz)

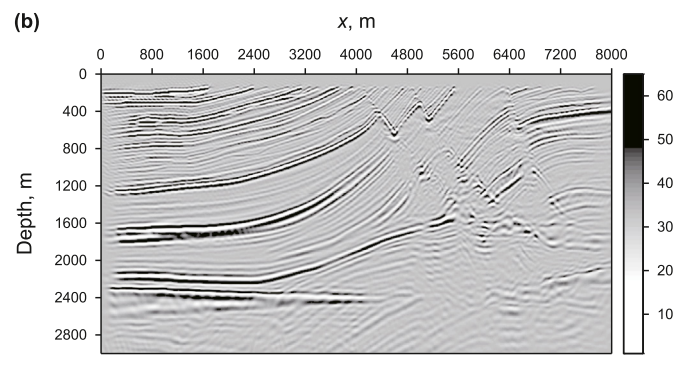
viscoacoustic data are unsatisfactory. This is because the conventional acoustic GSP algorithm lacks attenuation compensation terms, leading to severe waveform distortion resulting in reduced resolution in the migration results and weaker imaging energy in the deeper sections.

Further analysis of the waveforms in Figs. 6(b) and 7(b) reveals that the migration results of the acoustic GSP based on viscoacoustic data not only exhibit amplitude attenuation but also phase dispersion. These effects are primarily due to its viscoacoustic properties of subsurface structures, leading inaccurate migration results. Subsequently, the normalized average wavenumber spectra of imaging results are analyzed as shown in Fig. 8, it further indicates that the spectral curve of viscoacoustic GSP based on viscoacoustic data closely matches the spectral curve of acoustic GSP based on acoustic data, demonstrating significant compensation effects in the wavenumber band. Moreover, the spectral curve of acoustic GSP based on viscoacoustic data loses a substantial amount of amplitude energy, leading to its unsatisfactory imaging results. This further shows the meaningful compensation effect of viscoacoustic GSP. When considering viscoacoustic nature of the medium, it is imperative to use the corresponding viscoacoustic GSP for accurate migration results.

3.3. Marmousi model

To assess the attenuation compensation performance of our proposed algorithm, we perform imaging on the Marmousi model. Fig. 9 represents the Marmousi velocity model and its corresponding Q model (simulated using an empirical formula $Q=10.73\times v^{3.85}$), with detailed model parameters listed in Table 3.





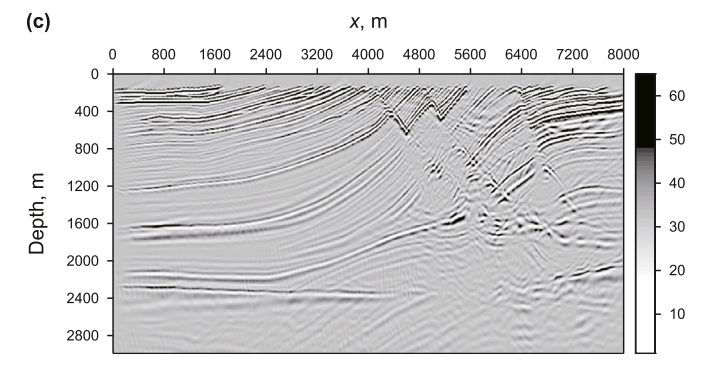


Fig. 10. Migration results: **(a)** acoustic GSP based on acoustic data, **(b)** viscoacoustic GSP based on viscoacoustic data, **(c)** acoustic GSP based on viscoacoustic data.

This model includes multiple complex features such as faults and

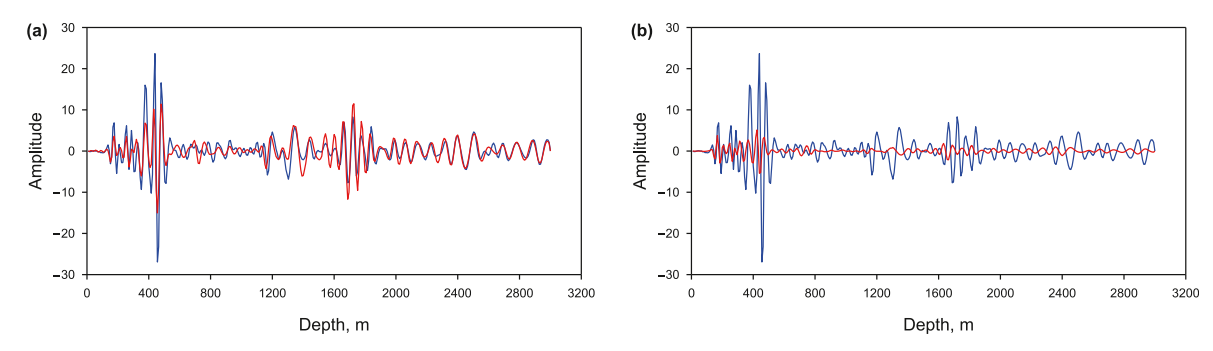


Fig. 11. Comparison of waveforms at x = 4800 m. **(a)** Illustration of viscous compensation effect (blue line: acoustic GSP based on acoustic data, red line: viscoacoustic GSP based on viscoacoustic data). **(b)** Illustration without compensation (blue line: acoustic GSP based on acoustic data, red line: acoustic GSP based on viscoacoustic data).

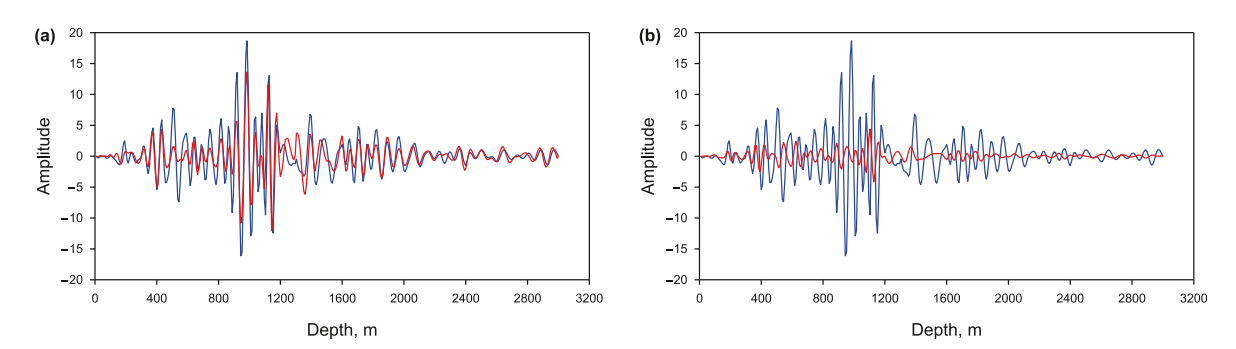


Fig. 12. Comparison of waveforms at x = 5600 m, (a) and (b) same as in Fig. 11.

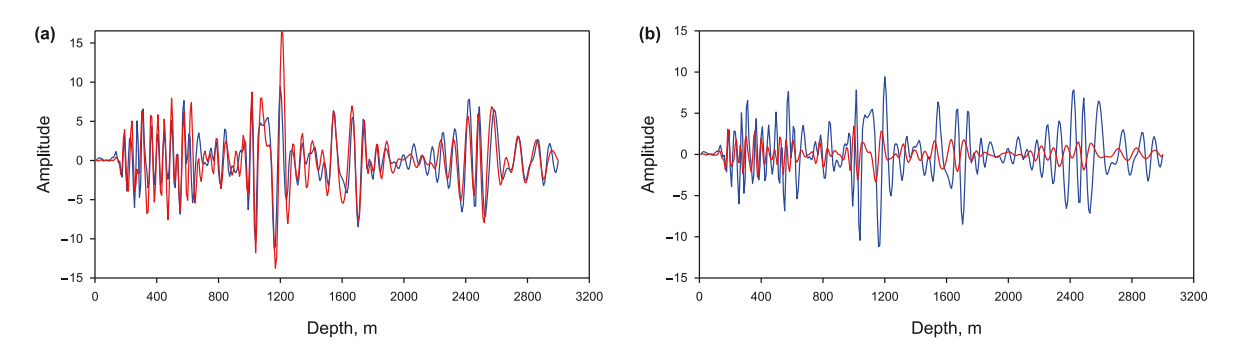


Fig. 13. Comparison of waveforms at x = 6400 m, (a) and (b) same as in Fig. 11.

anticlines. Two algorithms, acoustic GSP and viscoacoustic GSP, are employed to implement wavefield extrapolation and perform prestacked depth migration, respectively. The final imaging results are displayed in Fig. 10, which reveals that the imaging results from viscoacoustic GSP based on viscoacoustic data are in good agreement with acoustic GSP based on acoustic data. Above two algorithms accurately image the real subsurface structure of the Marmousi model, imaging its details clearly, as demonstrated in Fig. 10(a) and (b). Fig. 10(c) demonstrates that the migration results obtained from the viscoacoustic data-based acoustic GSP exhibit weaker imaging energy in deep and complex structures, accompanied by a significant reduction in resolution. To visually illustrate the compensation effecting of viscoacoustic GSP, we selected waveforms at x = 4800 m, x = 5600 m, and x = 6400 m for comparison, as depicted in Figs. 11-13. From the Figs. 11-13, it is obviously that, for the Marmousi model, the waveforms obtained by viscoacoustic GSP based on viscoacoustic data closely similar

with the waveforms from acoustic GSP based on acoustic data. Conversely, the result of acoustic GSP based on viscoacoustic data, display severely distorted seismic waveform information, making them inaccurate. Subsequently, the normalized average wavenumber spectra of the imaging results are analyzed. As shown in Fig. 14, it reveals that the viscoacoustic GSP based on viscoacoustic data exhibits wavenumber characteristics closely matching those of acoustic GSP based on acoustic wave data, with notable compensation effects in the wavenumber band. In contrast, the result of acoustic GSP based on viscoacoustic data loses more amplitude information, with the loss being most severe at medium and high wavenumbers, which is the main reason for the unsatisfactory imaging results. This conclusion is consistent with the findings from the 2D multi-layer model. It indicates that the viscoacoustic GSP is practical and has a certain level of accuracy for a complex model.

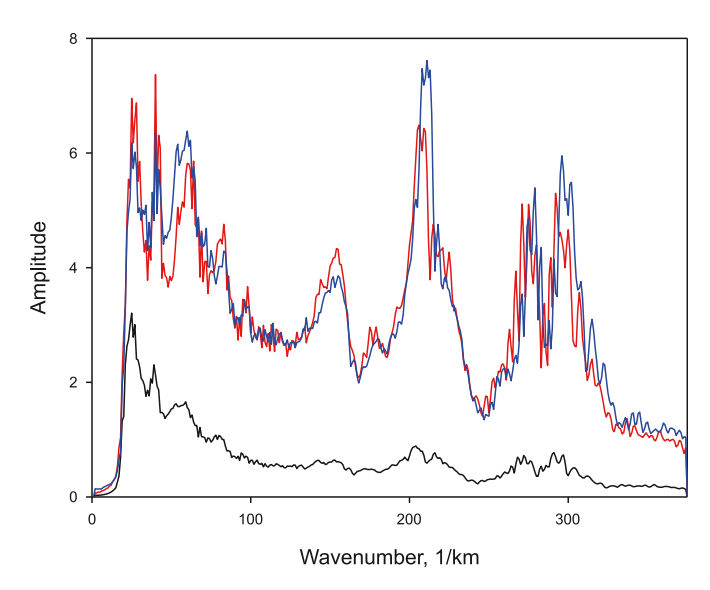


Fig. 14. Normalized average wavenumber spectra of imaging images along the vertical direction: the blue line is calculated by acoustic GSP based on acoustic data, the red line is calculated by viscoacoustic GSP based on viscoacoustic data, and the black line is calculated by acoustic GSP based on viscoacoustic data. All spectral curves are normalized to a reference spectral, which is the spectrum of the acoustic migration from acoustic data, without any attenuation.

3.4. Real seismic data

Our proposed method is applied to a set of actual seismic data. Fig. 15 shows the velocity model for the real data along with the Q model (calculated by $Q=9.83\times\nu^{2.85}$). Detailed parameters are listed in Table 4. Two algorithms, acoustic GSP and viscoacoustic GSP, are employed to implement wavefield extrapolation and perform migration, respectively. The final imaging results are presented in Fig. 16, demonstrating that both viscoacoustic GSP and acoustic GSP accurately image the subsurface structures. Moreover, in the regions highlighted by the red boxes, the results obtained by acoustic GSP are inferior to viscoacoustic GSP. Intuitively, the imaging events of viscoacoustic GSP is significantly thinner than that of acoustic GSP imaging events.

Further spectral analysis of the results between the two methods, is shown in Fig. 17. We observed the viscoacoustic GSP effectively compensates for the amplitude information loss by acoustic GSP in the low-wavenumber range and also provides noticeable compensation in the mid to high-wavenumber range.

Table 4 Forward modeling parameters for real seismic data.

Parameter	Value
Size, m	$4000(z) \times 15850(x)$
Reference frequency, Hz	1
Shot gather number	234
Source interval, m	60
Receiver number	360
Receiver interval, m	12.5
Minimum offset, m	0
Maximum offset, m	4500
Sampling length, s	5.00
Grid spacing, m	$5(z) \times 12.5(x)$
Sampling interval, s	0.002
Source type	Ricker wavelet (dominant frequency of 10 Hz)

This is the reason why viscoacoustic GSP outperforms acoustic GSP in terms of imaging quality. This shows that our proposed method has practical value, and its imaging performance for actual seismic data is better compared to acoustic GSP in certain regions.

3.5. Computational efficiency analysis

In our numerical experiments, it is worthy to compare the computational efficiency of our proposed method and the *Q*-RTM method. The detailed configuration of the computing environment is listed in the Table 5.

Fig. 18 shows the imaging results of *Q*-RTM (Zhu and Harris, 2014). *Q*-RTM is the most widely used migration method, and the superior imaging performance of *Q*-RTM is demonstrated compared to our proposed method. Therefore, the imaging results of *Q*-RTM are shown only for reference. For the two-dimensional multi-layer model, the imaging results of the *Q*-RTM method are generally consistent with our proposed method. However, for complex geological structures, it is evident that *Q*-RTM demonstrates better imaging performance on the Marmousi model. It's noteworthy that, the imaging results of *Q*-RTM method are basically consistent with our proposed method for the real seismic data.

Additionally, we compared the computational efficiency of our proposed viscoacoustic GSP method with Q-RTM. Table 6 provides a comparison of the computation time for calculating only the one shot gather using these above methods. The results clearly indicate that, compared to Q-RTM, the viscoacoustic GSP method has a significant advantage in computational efficiency. That's why we continue to focus on the development of one-way wave methods.

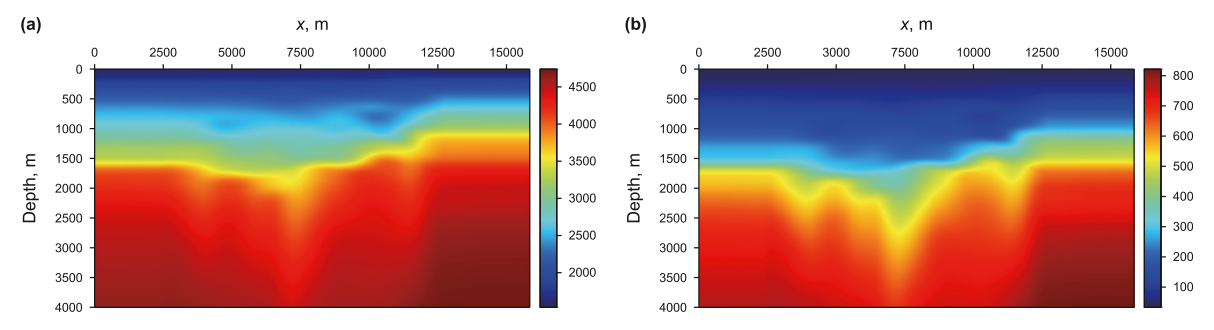


Fig. 15. (a) Velocity model, (b) Q model of real seismic data.

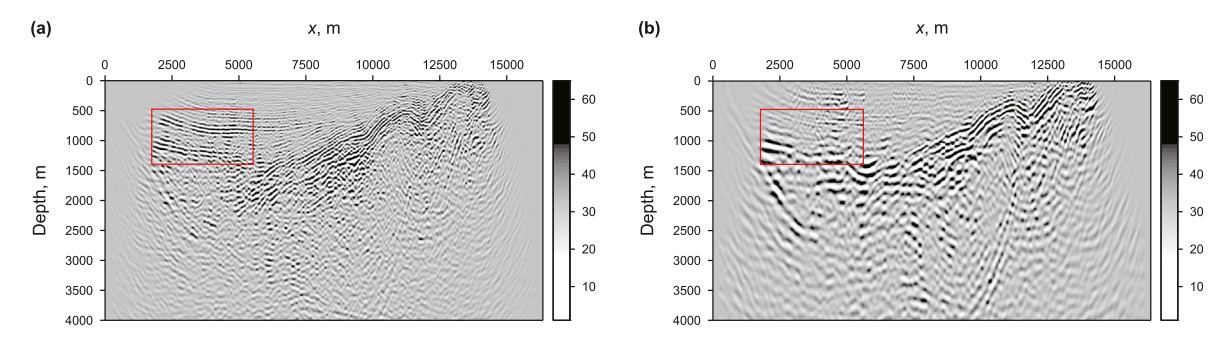


Fig. 16. Migration results: (a) viscoacoustic GSP based on real seismic data, (b) acoustic GSP based on real seismic data.

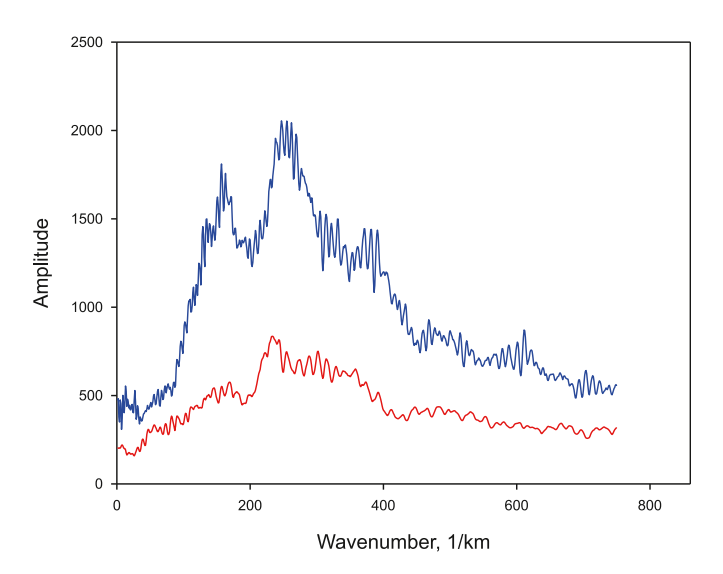


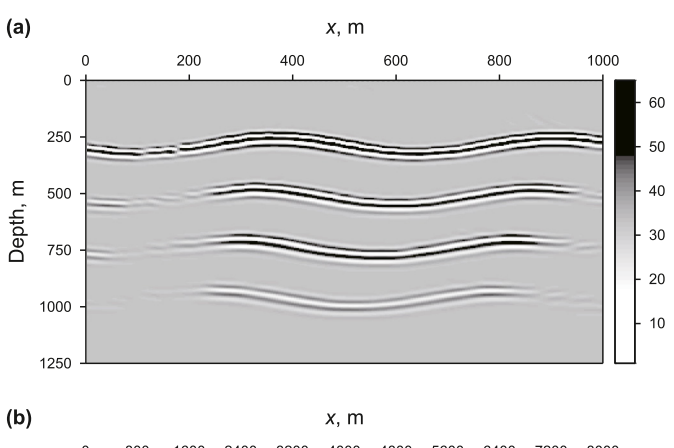
Fig. 17. Average wavenumber spectra of imaging images along the vertical direction: the blue line is calculated by viscoacoustic GSP using real seismic data, the red line is calculated by acoustic GSP using real seismic data.

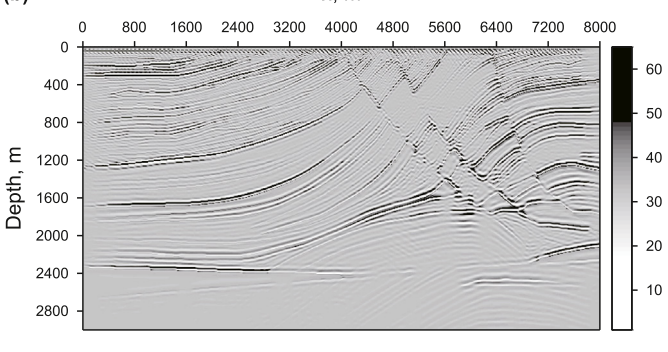
Table 5 Computing environment.

Component	Specification	Operating system	Software	Memory, G
CPU	AMD Ryzen 9 3950X	Windows 10	MATLAB	128

4. Conclusion

The conventional acoustic GSP migration, by neglecting the viscoelastic properties of subsurface medium, results in lower resolution of the migration. In real cases, it might severely affect seismic interpretation. To address this issue, we build upon the conventional acoustic GSP and incorporated viscoacoustic parameters to better capture subsurface information, proposing a GSP based on the VWE. Numerical experiments on two-dimensional multi-layer model and Marmousi model show that our proposed method can enhance the resolution of imaging. The viscoacoustic GSP proposed based on the viscoacoustic data is effective in obtaining imaging results comparable to the conventional acoustic GSP based on acoustic data. The application to actual seismic data underscores its significance and further confirms its practical value. It enhances imaging resolution, preserving the wavefield information to a greater extent and significantly improving the quality of deep subsurface imaging. Finally, we compared the computational





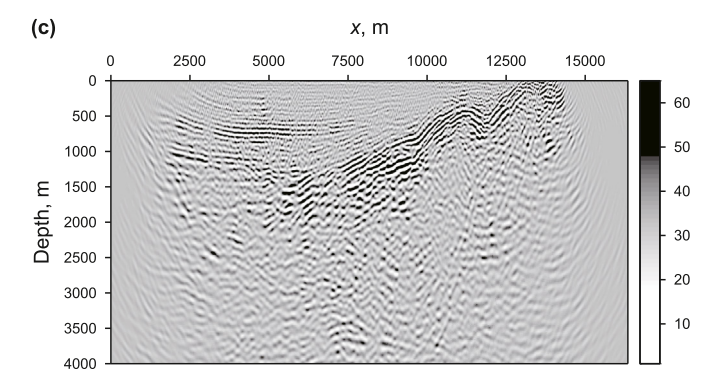


Fig. 18. Migration results using Q-RTM of **(a)** two-dimensional multi-layer model, **(b)** Marmousi model, **(c)** real seismic data.

efficiency of viscoacoustic GSP and Q-RTM. Despite Q-RTM demonstrating superior imaging performance, viscoacoustic GSP remains valuable due to its higher computational efficiency. This method represents an advancement in the development of wave equation migration theory.

Table 6Comparison of running time between viscoacoustic GSP method and Q-RTM method.

	Viscoacoustic GSP, s	Q-RTM, s
2D multi-layer model	2.046247	49.225586
Marmousi model	14.430469	388.962880
Real seismic data	81.056486	2585.835522

CRediT authorship contribution statement

Zhong-Kui Dai: Writing — review & editing, Writing — original draft, Visualization, Validation, Software, Investigation, Data curation, Conceptualization. **Jia-Chun You:** Writing — review & editing, Validation, Supervision, Resources, Project administration, Methodology, Funding acquisition, Formal analysis, Conceptualization. **Xing-Guo Huang:** Supervision. **Wei Liu:** Supervision.

Declaration of competing interest

The authors declare that they have no known competing financial interests or personal relationships that could have appeared to influence the work reported in this paper.

Acknowledge

We thank editors and reviewers for their valuable and constructive suggestions, which greatly improved the manuscript. This research is financially supported by the National Natural Science Foundation of China (grant Nos. 42004103, 42374149), Sichuan Science and Technology Program (grant No. 2023NSFSC0257) and CNPC Innovation Found (2022DQ02-0306).

Appendix A

The viscoacoustic GSP considering only the dispersion term

When considering only the dispersion effect in viscoacoustic wave equation, Eq. (19) simplifies to

$$-\omega^2 P(x,z;\omega) = \omega^{2\gamma} c^2 \omega_0^{-2\gamma} \cos(\pi \gamma) \nabla^2 P(x,z;\omega)$$
 (A-1)

Based on the previous derivation from Eq. (2) to Eq. (6), the corresponding vertical wavenumbers k_z and k_{z0} considering only the dispersion effect are defined as

$$k_{z} = \sqrt{\frac{\omega^{2}}{\nu^{2}(x, z_{i})}} \frac{1}{\cos(\pi \gamma)} \left(\frac{\omega}{\omega_{0}}\right)^{-2\gamma} + \frac{\partial^{2}}{\partial x^{2}}$$

$$k_{z0} = \sqrt{\frac{\omega^{2}}{c^{2}}} \frac{1}{\cos(\pi \gamma_{0})} \left(\frac{\omega}{\omega_{0}}\right)^{-2\gamma_{0}} + \frac{\partial^{2}}{\partial x^{2}}$$
(A-2)

Assuming
$$v_{\gamma,\cos}(x,z_i) = v(x,z_i) \times \left(\frac{\omega}{\omega_0}\right)^{\gamma} \sqrt{\cos(\pi\gamma)}$$
, $c_{\gamma_0,\cos} = c \times \left(\frac{\omega}{\omega_0}\right)^{\gamma_0} \sqrt{\cos(\pi\gamma_0)}$, The vertical wavenumbers k_z considering only the dispersion effect and the reference vertical wavenumbers k_{z0} can be simplified to

$$k_{z} = \sqrt{\frac{\omega^{2}}{\nu_{\gamma,\cos}^{2}(x,z_{i})} + \frac{\partial^{2}}{\partial x^{2}}}$$

$$k_{z0} = \sqrt{\frac{\omega^{2}}{c_{\gamma_{0},\cos}^{2}} + \frac{\partial^{2}}{\partial x^{2}}}$$
(A-3)

It can be observed that Eq. (A-3) is formally identical to Eq. (9), so the derivation process of the dispersive part of the viscoacoustic GSP is the same as the derivation of the conventional acoustic GSP. Therefore, the derived dispersive viscoacoustic one-way wave GSP is identical in form to the full viscoacoustic one-way wave GSP in Eq. (18), with the velocity term simplified as follows: $v_{\gamma}(x, z_i) = v_{\gamma,\cos}(x, z_i), c_{\gamma_0} = c_{\gamma_0,\cos}$.

Appendix B

The viscoacoustic GSP considering only the attenuation term

Only the attenuation effect is considered in viscoacoustic wave equation, and Eq. (19) is simplified as

$$-\omega^{2}P(x,z;\omega) = c\nabla^{2}p + \omega^{2\gamma}c^{2}\omega_{0}^{-2\gamma}i\sin(\pi\gamma)\nabla^{2}P(x,z;\omega)$$
 (B-1)

The vertical wavenumbers k_Z and the reference wavenumbers k_{Z0} , considering only the attenuation effect, are defined as

$$k_{z} = \sqrt{\frac{\omega^{2}}{v^{2}(x, z_{i})} \left(\frac{1}{1 + \omega^{2\gamma} \omega_{0}^{-2\gamma} i \sin(\pi \gamma)}\right) + \frac{\partial^{2}}{\partial x^{2}}}$$

$$k_{z0} = \sqrt{\frac{\omega^{2}}{c^{2}} \left(\frac{1}{1 + \omega^{2\gamma_{0}} \omega_{0}^{-2\gamma_{0}} i \sin(\pi \gamma_{0})}\right) + \frac{\partial^{2}}{\partial x^{2}}}$$
(B-2)

Assuming $v_{\gamma,\sin}(x, z_i) = v(x, z_i)\sqrt{1 + \omega^{2\gamma}\omega_0^{-2\gamma}i\sin(\pi\gamma)}$, $c_{\gamma_0,\sin} = c\sqrt{1 + \omega^{2\gamma_0}\omega_0^{-2\gamma_0}i\sin(\pi\gamma_0)}$, the vertical wavenumbers k_z considering only the attenuation effect and the reference vertical wavenumbers k_{z0} can be simplified to

$$k_{z} = \sqrt{\frac{\omega^{2}}{v_{\gamma,\sin}^{2}(x,z_{i})} + \frac{\partial^{2}}{\partial x^{2}}}$$

$$k_{z0} = \sqrt{\frac{\omega^{2}}{c_{\gamma_{0},\sin}^{2}} + \frac{\partial^{2}}{\partial x^{2}}}$$
(B-3)

Similarly, considering only the attenuation effect, the derivation process of the attenuated part of the viscoacoustic GSP follows the same steps as the derivation of the conventional acoustic GSP operator. Therefore, the resulting attenuated viscoacoustic oneway wave GSP has the same form as Eq. (18), with the velocity term simplified as follows: $v_{\gamma}(x,z_i) = v_{\gamma,\sin}(x,z_i), c_{\gamma_0} = c_{\gamma_0,\sin}$.

Appendix C

Stability analysis

The equation for wavefield propagation is as follows:

$$P(x, z + \Delta z; \omega) = e^{\pm ik_z \Delta z} P(x, z; \omega)$$
 (C-1)

where the definition of k_z has been provided by Eq. (8), and k_z can be expressed in the following form:

$$k_{z} = k_{r} + k_{i} \cdot i \tag{C-2}$$

where $i=\sqrt{-1}$ represents for imaginary unit, $k_{\rm r}$ represents the phase dispersion, and $k_{\rm i}$ represents the amplitude attenuation. It should be noted that, in the acoustic one-way wave equation depth migration, only the real part of k_z is retained to suppress the evanescent wave. While the imaginary part of k_z in the

viscoacoustic medium is associated with viscoacoustic effects.

Substitute Eq. (C-2) into Eq. (C-1), we can get downgoing/receiver wavefield:

$$P(x, z + \Delta z; \omega) = e^{ik_z \Delta z} P(x, z; \omega) = e^{ik_r \Delta z} e^{-k_i \Delta z} P(x, z; \omega)$$
 (C-3)

and upgoing/shot wavefield:

$$P(x, z + \Delta z; \omega) = e^{-ik_z \Delta z} P(x, z; \omega) = e^{-ik_r \Delta z} e^{k_i \Delta z} P(x, z; \omega)$$
 (C-4)

Based on Eqs. (C-3) and (C-4), we can simulate the attenuation of the up/down-going wavefield, and we can also use the operator $e^{k_i\Delta z}$ or $e^{-k_i\Delta z}$ to compensate the amplitude of the attenuated up or down-going wavefield.

Certainly, the imaginary part poses numerical stability challenges. To address this issue, we using the frequency wavenumber filter based on the maximum attenuation coefficient α introduced by Kjartansson (1979):

$$\alpha = \tan\left(\frac{\pi\gamma}{2}\right)\frac{\omega}{c_{\rm p}}\tag{C-5}$$

$$c_{\rm p} = v \left(\frac{\omega}{\omega_0}\right)^{\gamma} \tag{C-6}$$

Then, the frequency-wavenumber filter for suppressing the unreasonable amplitudes can be written as

$$k_{\rm i} = \left\{ \begin{array}{ll} k_{\rm i} & |k_{\rm i}| \leq \max(\alpha) \\ \\ 0 & |k_{\rm i}| > \max(\alpha) \end{array} \right. \tag{C-7}$$

References

- Bai, J., Chen, G., Yingst, D., Leveille, J., 2013. Attenuation compensation in viscoacoustic reserve-time migration. In: 83rd Annual International Meeting. SEG Expanded Abstracts, pp. 3825–3830. https://doi.org/10.1190/segam2013-1252.1.
- Baysal, E., Kosloff, D.D., Sherwood, J.W., 1983. Reverse time migration. Geophysics 48 (11), 1514–1524. https://doi.org/10.1190/1.1441434.
- Carcione, J.M., 2009. Theory and modeling of constant-Q P-and S-waves using fractional time derivatives. Geophysics 74 (1), T1–T11. https://doi.org/10.1190/13008548
- Carcione, J.M., Cavallini, F., Mainardi, F., Hanyga, A., 2002. Time-domain modeling of constant-Q seismic waves using fractional derivatives. Pure Appl. Geophys. 159, 1719—1736. https://doi.org/10.1007/s00024-002-8705-z.
- Carcione, J.M., Kosloff, D., Kosloff, R., 1988. Wave propagation simulation in a linear viscoelastic medium. Geophys. J. Int. 95 (3), 597–611. https://doi.org/10.1111/j.1365-246X.1988.tb06706.x.
- Chen, C., Yang, J.D., Mu, X.R., Li, Z.C., Huang, J.P., 2023. 2D Q-compensated multi-component elastic Gaussian beam migration. Petrol. Sci. 20 (1), 230–240. https://doi.org/10.1016/j.petsci.2022.09.019.
- Chen, H., Zhou, H., Li, Q., Wang, Y., 2016. Two efficient modeling schemes for fractional Laplacian viscoacoustic wave equation. Geophysics 81 (5), T233—T249. https://doi.org/10.1190/geo2015-0660.1.
- Claerbout, J.F., 1985. Imaging the Earth's Interior, vol. 1. Blackwell Scientific Publications Oxford.
- Dai, N., West, G.F., 1994. Inverse Q migration. In: 64th Annual International Meeting. SEG Expanded Abstracts, pp. 1418–1421. https://doi.org/10.1190/1.1822799.
- de Hoop, M.V., Le Rousseau, J.H., Wu, R.S., 2000. Generalization of the phase-screen approximation for the scattering of acoustic waves. Wave Motion 31 (1), 43–70. https://doi.org/10.1016/S0165-2125(99)00026-8.
- Dutta, G., Schuster, G.T., 2014. Attenuation compensation for least-squares reverse time migration using the viscoacoustic-wave equation. Geophysics 79 (6), S251–S262. https://doi.org/10.1190/geo2013-0414.1.
- Dvorkin, J.P., Mavko, G., 2006. Modeling attenuation in reservoir and nonreservoir rock. Lead. Edge 25 (2), 194–197. https://doi.org/10.1190/1.2172312.
- Fathalian, A., Trad, D.O., Innanen, K.A., 2020. An approach for attenuation-compensating multidimensional constant-Q viscoacoustic reverse time migration. Geophysics 85 (1), S33–S46. https://doi.org/10.1190/geo2019-0107.1.
- Futterman, W.I., 1962. Dispersive body waves. J. Geophys. Res. 67 (13), 5279–5291. https://doi.org/10.1029/JZ067i013p05279.

- Gazdag, J., 1978. Wave equation migration with the phase-shift method. Geophysics 43 (7), 1342–1351. https://doi.org/10.1190/1.1440899.
- Gazdag, J., Sguazzero, P., 1984. Migration of seismic data by phase shift plus interpolation. Geophysics 49 (2), 124–131. https://doi.org/10.1190/1.1441643.
- Grimbergen, J.L., Dessing, F.J., Wapenaar, K., 1998. Modal expansion of one-way operators in laterally varying media. Geophysics 63 (3), 995–1005. https://doi.org/10.1190/1.1444410.
- Groby, J.P., Tsogka, C., 2006. A time domain method for modeling viscoacoustic wave propagation. J. Comput. Acoust. 14 (2), 201–236. https://doi.org/10.1142/S0218396X06003001.
- He, R., Yang, W., Wang, E., Wei, X., Xie, C., Yan, G., 2019. Generalized screen propagator migration based on particle swarm optimization and amplitude-preserved imaging conditions. Oil Geophys. Prospect. 54 (4), 814–825. https://doi.org/10.13810/j.cnki.issn.1000-7210.2019.04.012 (in Chinese).
- Kim, B.Y., Seol, S.J., Lee, H.Y., Byun, J., 2016. Prestack elastic generalized-screen migration for multicomponent data. J. Appl. Geophys. 126, 116–127. https:// doi.org/10.1016/j.jappgeo.2016.01.016.
- Kjartansson, E., 1979. Constant Q-wave propagation and attenuation. J. Geophys. Res. Solid Earth 84 (B9), 4737–4748. https://doi.org/10.1029/JB084iB09p04737.
- Le Rousseau, J.M.H., de Hoop, M.V., 2001. Modeling and imaging with the scalar generalized-screen algorithms in isotropic media. Geophysics 66 (5), 1551–1568. https://doi.org/10.1190/1.1487101.
- Li, Q., 1993. High Resolution Seismic Data Processing. Petroleum Industry Press.
- Li, Z.C., Qu, Y.M., 2022. Research progress on seismic imaging technology. Petrol. Sci. 19 (1), 128–146. https://doi.org/10.1016/j.petsci.2022.01.015.
 Liao, Q., McMechan, G.A., 1996. Multifrequency viscoacoustic modeling and inver-
- Liao, Q., McMechan, G.A., 1996. Multifrequency viscoacoustic modeling and inversion. Geophysics 61 (5), 1371–1378. https://doi.org/10.1190/1.1444060.
- Liu, H.P., Anderson, D.L., Kanamori, H., 1976. Velocity dispersion due to anelasticity; implications for seismology and mantle composition. Geophys. J. Int. 47 (1), 41–58. https://doi.org/10.1111/j.1365-246X.1976.tb01261.x.
- Liu, L., Zhang, J., 2006. 3D wavefield extrapolation with optimum split-step Fourier method. Geophysics 71 (3), T95-T108. https://doi.org/10.1190/1.2197493.
- Lomnitz, C., 1957. Linear dissipation in solids. J. Appl. Phys. 28 (2), 201–205. https://doi.org/10.1063/1.1722707.
- McMechan, G.A., 1983. Migration by extrapolation of time-dependent boundary values. Geophys. Prospect. 31 (3), 413–420. https://doi.org/10.1111/j.1365-2478.1983.tb01060.x.
- Mittet, R., Sollie, R., Hokstad, K., 1995. Prestack depth migration with compensation for absorption and dispersion. Geophysics 60 (5), 1485—1494. https://doi.org/10.1190/1.1443882.
- Mu, X.R., Mao, Q., Huang, J.P., 2023. Stable attenuation-compensated reverse time migration and its application to land seismic data. Petrol. Sci. 20 (5), 2784–2795. https://doi.org/10.1016/j.petsci.2023.03.014.
- Mu, X., Huang, J., Yang, J., Li, Z., Ivan, M.S., 2022. Viscoelastic wave propagation simulation using new spatial variable-order fractional Laplacians. Bull. Seismol. Soc. Am. 112 (1), 48–77. https://doi.org/10.1785/0120210099.
- Mulder, W.A., Plessix, R.E., 2004. A comparison between one-way and two-way wave-equation migration. Geophysics 69 (6), 1491–1504. https://doi.org/ 10.1190/1.1836822.
- Qi, H., Greenhalgh, S., 2019. The generalized standard-linear-solid model and the corresponding viscoacoustic wave equations revisited. Geophys. J. Int. 219 (3), 1939–1947. https://doi.org/10.1093/gji/ggz407.
- Qi, H., Greenhalgh, S., 2022. Viscoacoustic wave equations for the power-law dependence of Q on frequency. Proceedings of the Royal Society A 478 (2260), 20220024. https://doi.org/10.1098/rspa.2022.0024.
- Qu, Y., Huang, C., Liu, C., Li, Z., 2020. Full-path compensated least-squares reverse time migration of joint primaries and different-order multiples for deep-marine environment. IEEE Trans. Geosci. Rem. Sens. 59 (8), 7109—7121. https://doi.org/ 10.1109/TGRS.2020.3024189.
- Qu, Y., Huang, J., Li, Z., Guan, Z., Li, J., 2017. Attenuation compensation in anisotropic least-squares reverse time migration. Geophysics 82 (6), S411–S423. https://doi.org/10.1190/geo2016-0677.1.
- Qu, Y., Li, Z., Guan, Z., Liu, C., Sun, J., 2021a. Topography-dependent Q-compensated least-squares reverse time migration of prismatic waves. IEEE Trans. Geosci. Rem. Sens. 60, 1–14. https://doi.org/10.1109/TGRS.2021.3125830.
- Qu, Y., Wang, Y., Li, Z., Liu, C., 2021b. Q least-squares reverse time migration based on the first-order viscoacoustic quasidifferential equations. Geophysics 86 (4), S283—S298. https://doi.org/10.1190/geo2020-0712.1.
- Qu, Y., Zhu, J., Chen, Z., Huang, C., Wang, Y., Liu, C., 2022. Q-compensated least-squares reverse time migration with velocity-anisotropy correction based on the first-order velocity-pressure equations. Geophysics 87 (6), S335–S350. https://doi.org/10.1190/geo2021-0689.1.
- Ristow, D., Rühl, T., 1994. Fourier finite-difference migration. Geophysics 59 (12), 1882–1893. https://doi.org/10.1190/1.1443575.
- Robertsson, J.O., Blanch, J.O., Symes, W.W., 1994. Viscoelastic finite-difference modeling. Geophysics 59 (9), 1444–1456. https://doi.org/10.1190/1.1443701.
- Schneider, W.A., 1978. Integral formulation for migration in two and three dimensions. Geophysics 43 (1), 49–76. https://doi.org/10.1190/1.1440828.
- Shin, S.I., Byun, J., Seol, S.J., 2015. Imaging tilted transversely isotropic media with a generalised screen propagator. Explor. Geophys. 46 (4), 349–358. https:// doi.org/10.1071/EG14113.
- Štekl, I., Pratt, R.G., 1998. Accurate viscoelastic modeling by frequency-domain finite differences using rotated operators. Geophysics 63 (5), 1779–1794. https:// doi.org/10.1190/1.1444472.
- Stoffa, P.L., Fokkema, J.T., de Luna Freire, R.M., Kessinger, W.P., 1990. Split-step

- fourier migration. Geophysics 55 (4), 410–421. https://doi.org/10.1190/
- Stolt, R.H., 1978. Migration by fourier transform. Geophysics 43 (1), 23–48. https://doi.org/10.1190/1.1440826.
- Strick, E., 1967. The determination of Q, dynamic viscosity and transient creep curves from wave propagation measurements. Geophys. J. Int. 13 (1–3), 197–218. https://doi.org/10.1111/j.1365-246X.1967.tb02154.x.
- Sun, J., Zhu, T., 2015. Stable attenuation compensation in reverse-time migration. In: 85th Annual International Meeting. SEG Expanded Abstracts, pp. 3942—3947. https://doi.org/10.1190/segam2015-5888552.1.
- Sun, J., Fomel, S., Zhu, T., Hu, J., 2016. Q-compensated least-squares reverse time migration using low-rank one-step wave extrapolation. Geophysics 81 (4), S271–S279. https://doi.org/10.1190/geo2015-0520.1.
- Sun, J., Zhu, T., Fomel, S., 2015. Viscoacoustic modeling and imaging using low-rank approximation. Geophysics 80 (5), A103—A108. https://doi.org/10.1190/geo2015-0083.1.
- Treeby, B.E., Cox, B.T., 2010. Modeling power law absorption and dispersion for acoustic propagation using the fractional Laplacian. J. Acoust. Soc. Am. 127 (5), 2741–2748. https://doi.org/10.1121/1.3377056.
- Treeby, B.E., Zhang, E.Z., Cox, B.T., 2010. Photoacoustic tomography in absorbing acoustic media using time reversal. Inverse Probl. 26 (11), 115003. https://doi.org/10.1088/0266-5611/26/11/115003.
- Valenciano, A.A., Chemingui, N., Whitmore, D., Brandsberg-Dahl, S., 2011. Wave equation migration with attenuation compensation. In: 12th International Congress of the Brazilian Geophysical Society, Rio de Janeiro, Brazil. https:// doi.org/10.3997/2214-4609-pdb.264.SBGF_2720.
- Wang, Y., 2008. Inverse-Q filtered migration. Geophysics 73 (1), S1–S6. https://doi.org/10.1190/1.2806924.
- Whitmore, N.D., 1983. Iterative depth migration by backward time propagation. In: 53rd Annual International Meeting. SEG Expanded Abstracts, pp. 382–385. https://doi.org/10.1190/1.1893867.
- Wu, R.S., 1994. Wide-angle elastic wave one-way propagation in heterogeneous media and an elastic wave complex-screen method. J. Geophys. Res. Solid Earth 99 (B1), 751–766. https://doi.org/10.1029/93JB02518.
- Wu, R.S., 2003. Wave propagation, scattering and imaging using dual-domain one-way and one-return propagators. Pure Appl. Geophys. 160, 509–539. https://doi.org/10.1007/PL00012548.
- Wu, R.S., Wang, Y., Gao, J., 2000. Beamlet migration based on local perturbation theory. In: 70th Annual International Meeting. SEG Expanded Abstracts, pp. 1008–1011. https://doi.org/10.1190/1.1815553.
- Xu, S.G., Bao, Q.Z., Ren, Z.M., 2023. Target-oriented Q-compensated reverse-time migration by using optimized pure-mode wave equation in anisotropic media. Petrol. Sci. 20 (2), 866–878. https://doi.org/10.1016/j.petsci.2022.12.016.
- Ye, Y., Zhuang, X., Hu, B., Li, Z., Chen, J., 2013. Synthesized plane wave preserved amplitude prestack depth migration based one-way wave equation. Oil Geophys. Prospect. 48 (5), 711–716. https://doi.org/10.13810/j.cnki.issn.1000-7210.2013.05.015 (in Chinese).

- You, J., Wu, R.S., Liu, X.W., et al., 2018b. Two-way wave equation-based depth migration using one-way propagators on a bilayer sensor seismic acquisition system. Geophysics 83 (3), S271–S278. https://doi.org/10.1190/geo2017-0172.1.
- You, J., Li, G., Liu, X., Han, W., Zhang, G., 2016. Full-wave-equation depth extrapolation for true amplitude migration based on a dual-sensor seismic acquisition system. Geophys. J. Int. 204 (3), 1462–1476. https://doi.org/10.1093/gji/ggv535.
- You, J., Liu, W., Huang, X., Xue, Y., Cao, J., 2023. Q-compensated wavefield depth extrapolation based migration using a viscoacoustic wave equation. Geophysics 89 (1), 1–69. https://doi.org/10.1190/geo2022-0542.1.
- You, J., Wu, R.S., Liu, X., 2018a. One-way true-amplitude migration using matrix decomposition. Geophysics 83 (5), S387–S398. https://doi.org/10.1190/ geo2017-0625.1.
- Yu, Y., Lu, R.S., Deal, M.M., 2002. Compensation for the effects of shallow gas attenuation with viscoacoustic wave-equation migration. In: 72nd Annual International Meeting. SEG Expanded Abstracts, pp. 2062–2065. https://doi.org/ 10.1190/1.1817107.
- Zhang, J.H., Wang, W.M., Wang, S.Q., Yao, Z.X., 2010a. Optimized Chebyshev Fourier migration: a wide-angle dual-domain method for media with strong velocity contrasts. Geophysics 75 (2), S23—S34. https://doi.org/10.1190/1.3350861.
- Zhang, J., Liu, L., 2007. Optimum split-step Fourier 3D depth migration: developments and practical aspects. Geophysics 72 (3), S167–S175. https://doi.org/10.1190/1.2715658.
- Zhang, J., Wapenaar, K., 2002. Wavefield extrapolation and prestack depth migration in anelastic inhomogeneous media. Geophys. Prospect. 50 (6), 629–643. https://doi.org/10.1046/j.1365-2478.2002.00342.x.
- Zhang, Y., Xu, S., Bleistein, N., Zhang, G., 2007. True-amplitude, angle-domain, common-image gathers from one-way wave-equation migrations. Geophysics 72 (1), S49–S58. https://doi.org/10.1190/1.2399371.
- Zhang, Y., Zhang, G., Bleistein, N., 2003. True amplitude wave equation migration arising from true amplitude one-way wave equations. Inverse Probl. 19 (5), 1113. https://doi.org/10.1088/0266-5611/19/5/307.
- Zhang, Y., Zhang, G., Bleistein, N., 2005. Theory of true-amplitude one-way wave equations and true-amplitude common-shot migration. Geophysics 70 (4), E1–E10. https://doi.org/10.1190/1.1988182.
- Zhang, Y., Zhang, P., Zhang, H., 2010b. Compensating for visco-acoustic effects in reverse-time migration. In: 70th Annual International Meeting. SEG Expanded Abstracts. pp. 3160–3164. https://doi.org/10.1190/1.3513503.
- Abstracts, pp. 3160–3164. https://doi.org/10.1190/1.3513503.

 Zhao, X.B., Zhou, H., Li, Q.Q., Wang, Y.F., 2017. A method to avoid the snapshots wavefields storage in reverse time migration. In: 79th EAGE Conference and Exhibition. EAGE Expanded Abstracts, pp. 1–5. https://doi.org/10.3997/2214-4609.201700679.
- Zhu, T., Harris, J.M., 2014. Modeling acoustic wave propagation in heterogeneous attenuating media using decoupled fractional Laplacians. Geophysics 79 (3), T105—T116. https://doi.org/10.1190/geo2013-0245.1.
- Zhu, T., Harris, J.M., Biondi, B., 2014. Q-compensated reverse-time migration. Geophysics 79 (3), S77–S87. https://doi.org/10.1190/geo2013-0344.1.